

# INTERANNUAL VARIABILITY OF SOUTHERN OCEAN CO<sub>2</sub> AND CFC FLUXES REVEALED FROM AN OGCM DRIVEN BY RE-ANALYSIS OCEAN CURRENTS

Valsala V<sup>1\*</sup>, S. Maksyutov<sup>1</sup> and M. Ikeda<sup>2</sup>

GOSAT, CGER, National Institute for Environmental Studies, Tsukuba, Japan.  
Graduate School of Earth System Sciences, Hokkaido University, Sapporo, Japan.

## 1. INTRODUCTION

A novel strategy to model air-sea CO<sub>2</sub> and CFC fluxes is designed by using a coupled physical-biogeochemical model. The physical part of the model is an offline transport model driven by assimilated ocean currents, temperature, salinity and other diagnostic physical parameters derived from the re-analysis data set of GFDL, Princeton (Valsala et al. 2008). The chemical part of the model is a one component inorganic chemistry derived from the OCMIP-II type Abiotic protocol. The ecosystem model is a one component phosphate dependent export production and re-mineralization after McKinley et al. (2004). The model is initialized with contemporary inventories of Dissolved Inorganic Carbon (DIC) from the GLODAP data set (Key et al. 2004). The advantages of this modeling system is that (a) the physical circulations are constrained by the observations in the assimilation processes and thereby chances of representing a realistic circulation (b) initialization from a contemporary inventories of DIC leading to relatively shorter spin-up simulations to study CO<sub>2</sub> cycle for a specific period of time (3) easier way of construction of adjoint model to assimilate observations using 4D-variational methods.

## 2. BIO-GEOCHEMICAL OGCM.

We use an Ocean General Circulation Model (OGCM) coupled with a simplified one component ecosystem model. The physical part of this model is an Offline Oceanic Tracer Transport Model (OTTM.1.0; hereafter OTTM) by Valsala et al. (2008) driven by re-analysis ocean currents, temperature, salinity and other physical parameters. In the OTTM, the ocean circulation, temperature and salinity are provided from a pre-calculated data archive. Here we use a 40- year ocean re-analysis data sets derived from the Geophysical Fluid Dynamics Laboratory. These data are made from Modular Ocean Model-4 (MOM4-SIS) ocean-ice component coupled with the Climate Model (CM2.1) with an assimilation of in situ temperature profiles from the National Oceanographic Data Center (NODC) archives using a 3D variational scheme (available at [http://nomads.gfdl.noaa.gov:9090/dods/GODAEOceanAssimilation/om3\\_sis\\_core\\_assim\\_v7c/](http://nomads.gfdl.noaa.gov:9090/dods/GODAEOceanAssimilation/om3_sis_core_assim_v7c/)).

The OTTM incorporates self operating diagnostic mode vertical mixing and sub-grid scale parameterizations because the coefficients for these processes are not readily available from the re-analysis data. So they are estimated within the model. The vertical mixing is a combination of the K-Profile Parameterization (KPP; Large et al. (1994)) and Bryan and Lewis (1979) type back ground vertical diffusion. The horizontal diffusions are a combination of flow dependent diffusion in which the coefficients are

proportional to the stress and strain experienced in the local fluid volume (Griffies and Hallberg, 2000) and advection fluxes due to eddy induced transports as in Gent and McWilliams (1990).

The horizontal advection is taken from the offline data archive while vertical velocities are found from mass conservation principles. The surface boundary exchanges the fresh water with the atmosphere as evaporation and precipitation which appear as velocities at the top cell face of the surface grid. The free-surface kinematic boundary condition is provided from the sea surface height taken from the re-analysis data. This model is used to find the CFC-11 cycle in Valsala et al. (2008).

The air-sea gas exchange depends upon the piston velocity  $K_w$  and the difference in partial pressure of CO<sub>2</sub> ( $p\text{CO}_2$ ) between the saturated surface ocean and the immediate atmosphere above the surface. Since we are primarily interested in the air-sea CO<sub>2</sub> flux response to changing physical forcing, a constant atmospheric  $p\text{CO}_2$  of 354  $\mu\text{atm}$  (a value observed in 1990) is applied. The air-sea flux is formulated as  $\text{GAS}_{\text{EX}} = K_w (p\text{CO}_{2\text{Atm}} - p\text{CO}_{2\text{Ocean}})$ . The piston velocity  $K_w$  is the turbulent velocity with which the gaseous CO<sub>2</sub> enters or leaves the surface ocean according to the wind-speed and CO<sub>2</sub> solubility conditions as formulated in the Wanninkhof (1992). We use the gas exchange proportionality constant  $a = 0.337$ . The surface wind-speed is composed of a 10 day average of a 4-hourly squared wind-speed which fully accounts for 4 hourly wind-speed variance ( $u_{10}^2 + \text{sig}^2 u_{10}$ ) where  $u_{10}$  is the wind-speed at 10 meter. The polar ice caps are used to partially mask the air-sea gas exchange in sea-ice conditions with a spatial map of ice index ranges from 0.2 to 1 as given in the OCMIP-II.

The ecosystem model is the same as that used in McKinley et al. (2004). In this model, the net primary production in the euphotic zone is found from the monthly maps of the phosphate and light availability and scaled it by a regional mask which stands for the iron limitation, grazing efficiency or recycling. The export production in the euphotic zone (0-140m) is formulated as  $B(z) = \alpha \cdot I / (I + I_0) \cdot P / (P + P_0)$ , where,  $\alpha$  represents the other controlling factors of the export rates. The values of the maximum export rate,  $\alpha$ , account for all the processes leading to export which are not represented by the explicit phosphate and light limitation (McKinley et al., 2004).

## 2.1 EXPERIMENTS AND METHODS

The model is simulated for the mean state of DIC (pre-run) using a monthly mean circulations and other physical parameters derived from 1975-1984 (i.e. 10 years). The pre-run of the model is initialized with an annual mean values of DIC derived from the

GLODAP data (Key et al., 2004). The pre-run is carried out for 20 years using a monthly mean circulations and the surface gas exchange forcing that are repeated at every year. The surface DIC concentration and air-sea CO<sub>2</sub> flux of the model reach a quasi-equilibrium state at the end of the first 10 years of the pre-run and continue with a minimum departure from the mean state thereafter. The average of the last five year simulation of the pre-run is taken as the restart condition of the interannual simulation. The model is started from the restart condition and run through the monthly fields of the year 1980 once and then continued the run from 1980 to 1999 using the real-time data. The model deviates from the restart condition as soon as the data of 1980 is introduced and a near steady state is reached by the time model pass one time through the fields of the year 1980.

### 3. AIR-SEA CO<sub>2</sub> FLUX

The global mean CO<sub>2</sub> flux of the model is constructed from 1980 to 1999. The global mean has a net sink of  $1.42 \pm 0.40 \text{ PgCyr}^{-1}$ . The model captures the major features of the global CO<sub>2</sub> flux such as the eastern tropical Pacific emission and the high latitude sinks with maximum amplitude in the north Atlantic.

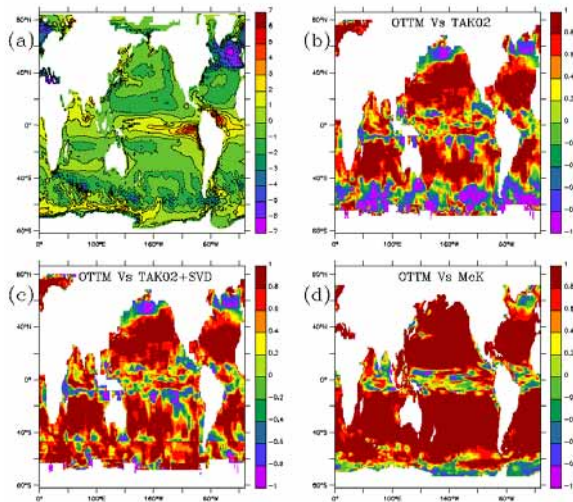


Figure 1: (a) 20 year mean (1980-1999) air-sea CO<sub>2</sub> flux simulation in mole/m<sup>2</sup>/year. Seasonal correlation of model vs (b) Takahashi (2002); (TAK02) and (c) Takahashi (2002) corrected with SVDX inversion. (d) Same as (a) but for model Vs McKinley et al. (2004).

### 4. SOUTHERN OCEAN (SO) CO<sub>2</sub> FLUX

Cross examining the seasonal cycle from various approaches such as observational based (TAK02, Metzl et al. (2006)), OGCM based (McKinley et al. (2004a); Wetzel et al. (2005); our study) and atmospheric inversion based (Roy et al. (2003); Gurney et al. (2004); Patra et al. (2005); our SVD method), we have reached an assessment of our model SO CO<sub>2</sub> flux as follows. (a) An annual mean CO<sub>2</sub> flux of SO for 1980-1999 should be more realistically about  $0.4 \text{ PgCyr}^{-1}$

(b) Our model maximum sink of SO CO<sub>2</sub> has an unrealistic lag of two months (i.e. toward June-July) and exaggerated sink for three months (i.e. July-Sept). (c) The SO seasonal cycle of our model is within the uncertainties of various observational based estimates.

### 4.1 INTERANNUAL VARIABILITY OF SOUTHERN OCEAN CO<sub>2</sub> FLUX.

Our study points out that the SO trend in the CO<sub>2</sub> flux is mostly located below 60°S. The Figure 2c shows that the SO's CO<sub>2</sub> emission gradually increases in the last two decades. The increasing trend of emission is most obvious in the south of 60°S (see Figure 2(d)). The maximum amplitude of the CO<sub>2</sub> emission south of 60°S is  $0.2 \text{ PgCyr}^{-1}$  from 1995 onwards. The CO<sub>2</sub> emission from the period 1993 to 1998 is larger than that of the period 1980 to 1993. This is consistent with the recent atmospheric inversion and OGCM simulations of Le-Quere et al. (2007). During the first half of our simulation, the average CO<sub>2</sub> emission from the south of 60°S is  $0.052 \text{ PgCyr}^{-1}$  while during the second half, it is increased to  $0.119 \text{ PgCyr}^{-1}$ . This shows a net increase of  $0.067 \text{ PgCyr}^{-1} \text{ decade}^{-1}$  which is close to the value of  $0.08 \text{ PgCyr}^{-1} \text{ decade}^{-1}$  reported in Le-Quere et al. (2007).

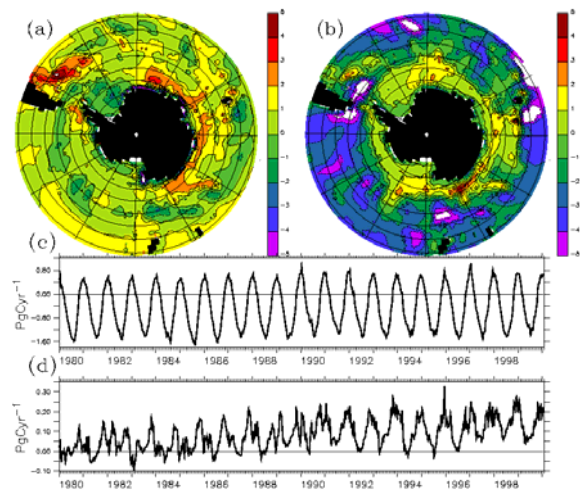


Figure 2: Air-sea CO<sub>2</sub> fluxes in (a) summer and (b) winter in mole/m<sup>2</sup>/year. (c) Area integrated CO<sub>2</sub> flux in PgC/year (d) Area integrated interannual anomalies of CO<sub>2</sub> flux for (60°S-90°S).

Figure 3(d) shows the area integral of CO<sub>2</sub> flux for the regions of 40°S to 60°S and 60°S to 90°S separately. The individual contribution of each of this region to the net CO<sub>2</sub> flux of the SO has an almost similar magnitude, even though the area occupied by the southern part is only 33.5% of the total area of the SO. This implies that the flux magnitude is larger in the south of 60°S than the rest of the SO. The interannual variability has nearly a zero trend in the area integral of 40°S to 60°S. This is because the regional positive and negative trends cancel each other as a whole. The corresponding pCO<sub>2</sub>

trend (see Figure 3(b)) shows similar features as that shown in the CO<sub>2</sub> flux.

The location of trends in the model close to the continent suggests two possible reasons, (1) an increase in surface wind causes an increase in upwelling and vertical mixing of DIC rich subsurface water and the subsequent increase in the surface ocean pCO<sub>2</sub> (2) the increase in addition of water fluxes including the melting of sea-ice influencing the alkalinity (ALK) and pH of the surface water and hence results in a increasing trend of CO<sub>2</sub> emission. However, the reason-1 may also bring an opposite effect on CO<sub>2</sub> emission (i.e. a reduced emission trend) because of surfacing of high saline water due to the enhanced upwelling which might result in a high alkalinity and shifting the CO<sub>2</sub> equilibrium toward a more air-to-sea flux. In order to separate the effects of different components of the carbonate chemistry on the net change in the pCO<sub>2</sub>, we have done a sensitivity analysis as follows.

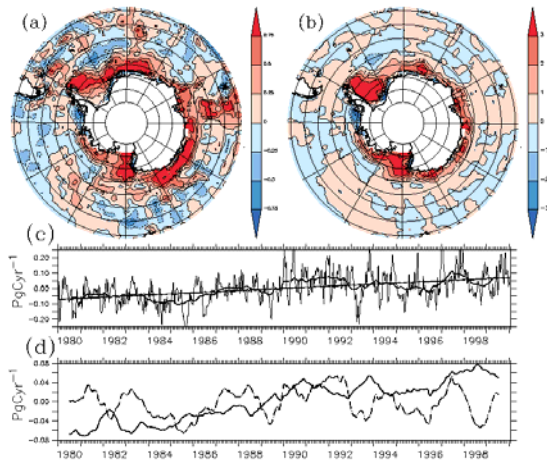


Figure 3: Trend in the SO CO<sub>2</sub> cycle. (a) 20-year trend of CO<sub>2</sub> flux (gCm<sup>-2</sup> yr<sup>-1</sup> yr<sup>-1</sup>). (b) 20-year trend of pCO<sub>2</sub> (µatmyr<sup>-1</sup>). (c) CO<sub>2</sub> flux anomalies integrated over the entire SO. A 12-month running average is overlaid. The trend line is shown. (d) Same as (c) but integrated over 400 S600 S (dash line) and 60°S-90°S (thin line). A 12-month running average is applied.

#### 4.2 INTERANNUAL VARIABILITY OF pCO<sub>2</sub> COMPONENTS.

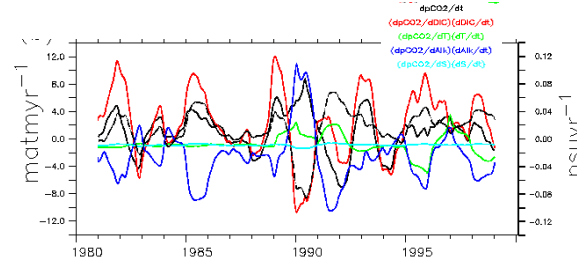
The dependencies of the surface ocean pCO<sub>2</sub> on DIC, Temperature, Alkalinity and Salinity can be assumed as a linear relation as given in TAK02, i.e.,

$$\frac{dpCO_2}{dt} = \frac{\partial pCO_2}{\partial DIC} \frac{dDIC}{dt} + \frac{\partial pCO_2}{\partial T} \frac{dT}{dt} + \frac{\partial pCO_2}{\partial ALK} \frac{dALK}{dt} + \frac{\partial pCO_2}{\partial S} \frac{dS}{dt}$$

Equation (1)

These components are calculated from the model's interannual variability. On the calculation of variability of each of the term, the other variables are kept constant

and the Abiotic carbon solubility pump model (i.e. Section 2, paragraph-4) is run separately using the model variability of DIC and data variability of



Temperature, Salinity and Alkalinity.

Figure 4: Components of total change of pCO<sub>2</sub> (µatmyr<sup>-1</sup>) interannual variability for the SO. A right-axis panel is for the interannual salinity trend (dash line). A 12-month running mean is applied twice to smooth the variability.

In the SO (Figure 4(b)), however, the dependency of pCO<sub>2</sub> on the component of alkalinity and DIC is comparable and complementary to each other. That means, a decreasing tendency of the pCO<sub>2</sub> due to the alkalinity changes is followed by an increasing tendency of the pCO<sub>2</sub> due to the DIC changes. However, the magnitude the former is only half the magnitude of the later (except for 1985 and 1990) and hence net pCO<sub>2</sub> variability in the south of the SO is determined by the variability of DIC brought by the circulation changes.

It is to be noted that the alkalinity is not transported within our model, but it is estimated from the re-analysis salinity inputs with a constant conversion factor of 2310 µequilibrium kg<sup>-1</sup> as given in OCMIP-II Abiotic run protocols (available at <http://www.ipsl.jussieu.fr/OCMIP/>) However, the salinity inputs from the re-analysis data contains the effect of transport, surface freshening and evaporation. The interannual tendency of salinity is also plotted in the bottom panel of Figure 4 (right axis; dash line). When the surface salinity increases and hence the alkalinity, the surface pCO<sub>2</sub> reduces because of more negative ions and higher pH values. At the same time the increase in the DIC contributes to a net increase in the pCO<sub>2</sub> regardless of the reduction of pCO<sub>2</sub> brought by the alkalinity changes, which is in fact, only half the magnitude of the DIC induced pCO<sub>2</sub> changes. The changes in the salinity, which is also in phase with the changes in the DIC, point out a source of high saline water from the subsurface through a strong upwelling. This can bring DIC rich subsurface water to the surface and can cause a large flux of CO<sub>2</sub>. This in fact points to the fact that the increasing trend in the SO winds and subsequent ocean mixing and circulation changes cause an increasing trend in the CO<sub>2</sub> flux emission. This is consistent with the findings of Wetzel et al. (2005) and Le-Quere et al. (2007). In our study we pointed out that this trend is most prominent in the polar continental margin than in the low latitude of the SO.

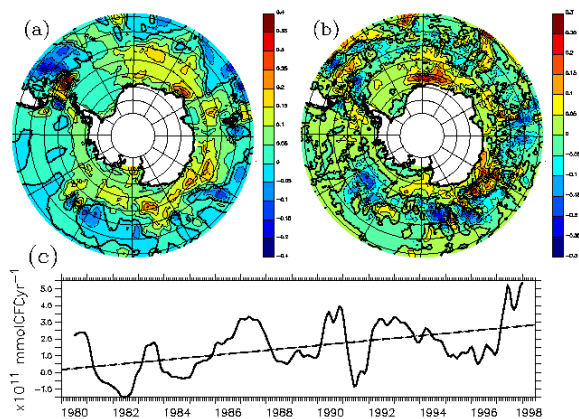


Figure 5: The SO CFC-11 flux (positive into the ocean). (a) 20-year means CFC flux in  $\mu\text{molCFCyr}^{-1}$ . (b) 20-year trend of CFC flux in  $\mu\text{molCFCyr}^{-1} \text{ yr}^{-1}$ . (c) Interannual variability of south of 600 S integrated CFC-11 flux anomalies in  $\mu\text{molCFCyr}^{-1}$ . A 12-month running mean is applied. The trend line is also shown.

#### 4.3 INTERANNUAL VARIABILITY OF CFC-11 FLUX.

The mean CFC flux in the SO has similarities with the corresponding  $\text{CO}_2$  fluxes. For instance, the southern part of the SO has a large sinking capacity for CFC which shows that the replenishing of the surface water by relatively old bottom water due to the Ekman divergence which causes an under-saturation of CFC-11 concentration in the surface. The colder upwelling of subsurface water also enhances this under-saturation and causes an enhanced flux of CFC-11 from air-to-sea. In the following analysis, we will see that this mechanism has a linear increasing trend in the last two decades. This region of high CFC-11 sink is closely correlated with the high  $\text{CO}_2$  source which is quite expected because of the surfacing of DIC rich subsurface water.

In the lower latitudes of the SO (i.e.  $40^\circ\text{S}$ - $60^\circ\text{S}$ ), the CFC has localized source regions where the  $\text{CO}_2$  has an annual mean sink. This source regions show the surfacing of relatively new Antarctic Intermediate Water (AAIW) and Antarctic Mode Water (AAMW) (which have relatively younger age of CFC-11) by means of vertical mixing. However, in the case of  $\text{CO}_2$  this mixing and overturning causes a surfacing of nutrient depleted euphotic zone water and reasons a reduced  $p\text{CO}_2$  and an enhanced  $\text{CO}_2$  sink. The interannual anomalies of the CFC flux from the SO (south of  $60^\circ\text{S}$ ) are shown in Figure 5(c). It clearly shows a gradual increase of CFC sink in the southern part of the SO. The trend line is also shown. During the last 20 years, the CFC sink in the SO has increased by an amount of  $2.9 \times 10^{11} \mu\text{molCFCyr}^{-1}$ . The reason for this increase is mainly due to the physical changes in the circulation. The increased amount of upwelling and surfacing of the deep water by mixing results in a low  $p\text{CFC}$  surface water and causes more addition of CFC from air-to-sea. However, in the case of DIC, this

surfacing of the deep water enriches the surface  $p\text{CO}_2$  and hence causes strong emission.

## 5 Results and Conclusion

A 20-year variability of the SO (south of  $40^\circ\text{S}$ )  $\text{CO}_2$  and CFC flux is investigated using an offline OGCM coupled with a Biogeochemical model driven by re-analysis ocean data sets. The model reproduces the climatological distribution of the global ocean sources and sinks of  $\text{CO}_2$  reasonably well and comparative with the observations of TAK02, the inversion-based estimates of Gurney et al. (2004); Patra et al. (2005) and other modeling results of Le-Quere et al. (2000); McKinley et al. (2004). The model reproduced a mean SO sink of  $0.46 \text{ PgCyr}^{-1}$ . An inversion of atmospheric  $\text{CO}_2$  using singular value decomposition techniques revealed that the SO observations of TAK02 need a flux correction of  $0.52 \text{ PgCyr}^{-1}$  out of the ocean. In the model, the SO  $\text{CO}_2$  flux anomalies show an emission trend of  $0.062 \text{ PgCyr}^{-1} \text{ decade}^{-1}$ . The interannual trend of  $\text{CO}_2$  source is found most prominent in the south of  $60^\circ\text{S}$ . The component analysis of  $p\text{CO}_2$  variability dependencies on DIC, ALK, temperature and salinity shows that the interannual  $p\text{CO}_2$  trends are driven by DIC changes brought by the changes in the circulation. This has been confirmed by the corresponding increasing trend in the CFC sink of the southern part of SO. It has been identified that the mean sinking flux of SO  $\text{CO}_2$  has no significant trend whereas the mean out gassing of  $\text{CO}_2$  has been increased linearly from 1980 through 1999.

## 6. References

- Bryan, K. and L. J. Lewis, 1979: A water mass model of the World ocean. *J. Geophys. Res.*, 84, 25032517.
- Gent, P. R. and J. C. McWilliams, 1990: Isopycnal mixing in Ocean circulation models. *J. Phys. Oceanogr.*, 20, 150155.
- Griffies, S. M. and R. W. Hallberg, 2000: Biharmonic friction with a smagorinsky-like viscosity for use in large-scale eddy-permitting ocean models. *J. Phys. Oceanogr.*, 128, 29352946.
- Gurney, K. R., R. M. Law, A. S. Denning, P. J. Rayner, B. Pak, and Transcom-3-L2-modelers, 2004: Transcom-3 inversion intercomparison: Control results for the estimation of seasonal carbon sources and sinks. *Global Biogeochem. Cycles*, 18, doi:10.1029/2003GB002111.
- Key, R. M., A. Kozyr, C. L. Sabine, K. Lee, R. Wanninkhof, J. L. Bullister, R. A. Feely, F. J. Millero, C. Mordy, and T.-H. Peng, 2004: A global ocean carbon climatology: Results from Global Ocean Data Analysis Project (GLODAP). *J. Geophys. Res.*, 18, doi:10.1029/2004GB002247.
- Large, W. G., J. C. McWilliams, and S. C. Doney, 1994: Ocean vertical mixing: A review and a model with a

nonlocal boundary layer parameterization. *Rev. Geophys.*, 32, 363403.

Le-Quere, C., C. Rodenbeck, E. T. Buitenhuis, T. J. Conway, R. L. .and A. Gomez, C. Labuschagne, M. Ramonet, T. Nakazawa, N. Metzl, N. Gillett, and M. Heimann, 2007: Saturation of the southern ocean CO<sub>2</sub> sink due to recent climate change. *Science* , 316, 1735-1738.

McKinley, G. A., M. J. Follows, and J. Marshall, 2004a: Mechanism of air-sea CO<sub>2</sub> flux variability in the equatorial Pacific and North Atlantic. *Global Biogeochem. Cycles* , 18, doi:10.1029/2003GB002179.

Metzl, N., C. Brunet, A. Jabaud-Jan, A. Poission, and B. Schauer, 2006: Summer and winter air-sea CO<sub>2</sub> fluxes in the southern ocean. *Deep-Sea Res.*, 53, 15481563.

Patra, P. K., S. Maksyutov, M. Ishizawa, T. Nakazawa, and T. T. abd J. Ukita, 2005: Interannual and decadal changes in the air-sea CO<sub>2</sub> flux from atmospheric CO<sub>2</sub> inverse modeling. *Global Biogeochem. Cycles* , 19, doi:10.1029/2004GB002257

Roy, T., P. Rayner, R. Matear, and R. Francey, 2003: Southern hemisphere ocean CO<sub>2</sub> uptake: reconciling atmospheric and oceanic estimates. *Tellus* , 55B, 701-710.

Takahashi, T., S. C. Sutherland, C. Sweeney, A. Poisson, N. Metzl, B. Tilbrook, N. Bates, R. Wanninkhof, R. A. Feely, C. Sabine, J. Olafsson, and Y. No jiri, 2002: Global sea-air CO<sub>2</sub> flux based on climatological surface ocean pCO<sub>2</sub> and seasonal biological and temperature effect. *Deep-Sea Res.*, 49, 16011622.

Valsala, K. V., S. Maksyutov, and M. Ikeda, 2008: Desing and validation of an offline oceanic tracer transport model for a carbon cycle study. *J. Climate* , 21, 27522769.

Wanninkhof, R., 1992: Relationship between wind speed and gas exchange over the ocean. *J. Geophys. Res.*, 97, 73737382.

Wetzel, P., A. Winguth, and E. Maier-Reimer, 2005: Sea to air CO<sub>2</sub> flux from 1948 to 2003: A model study. *Global Biogeochem. Cycles* , 19, doi:10.1029/2004GB002339.

---

\* Corresponding author address: Vinu Valsala, GOSAT, CGER, National Institute for Environmental Studies, 16-2 Onogawa, Tsukuba, Ibaraki, Japan  
e-mail: vinu.valsala@nies.go.jp